Physical characteristics and dynamics of the coastal Latex09 Eddy derived from in situ data and numerical modeling.

Marion Kersale, Anne Petrenko, Andrea M. Doglioli, I. Dekeyser, Francesco Nencioli

Physical characteristics and dynamics of the coastal Latex09 Eddy derived from *in situ* data and numerical modeling.

M. Kersalé,[1] A. A. Petrenko,[1] A. M. Doglioli,[1] I. Dekeyser,[1] F. Nencioli[1]

[1]Aix-Marseille Université, Université du Sud Toulon-Var, CNRS/INSU, IRD, MIO, UM 110, 13288, Marseille, Cedex 09, France.

Abstract.

We investigate the dynamics of a coastal anticyclonic eddy in the western part of the Gulf of Lion (GoL) in the northwestern Mediterranean Sea during the Latex campaign in the summer 2009 (Latex09). The sampling strategy combines SST satellite imagery, hull-mounted ADCP data, CTD casts and drifter trajectories. Our measurements reveal an anticyclonic eddy (*Latex09 eddy*) with a diameter of ~23 km and maximum depth of 31 m, centered at 3°34'E - 42°33'N. We use a high resolution, 3-dimensional, primitive equation numerical model to investigate its generation process and evolution. The model is able to reproduce the observed eddy, in particular its size and position. The model results suggest that the *Latex09 eddy* is induced by a large anticyclonic circulation in the northwestern part of the GoL, pushed and squeezed toward the coast by a meander of the Northern Current. This represents a new generation mechanism that has not been reported before. The post generation dynamics of the eddy is also captured by the model. The collision of the *Latex09 eddy* with Cape Creus results in a transient structure, which is depicted by the trajectories of two Lagrangian drifters during Latex09. The transient structure and its advection lead to a transfer of mass and vorticity from the GoL to the Catalan shelf, indicating the importance of mesoscale structures in modulating such exchanges in the region.

Keywords: Coastal eddies, *in situ* measurements, numerical modeling, mesoscale, Gulf of Lion.

1. Introduction

Continental shelf processes are often affected by large eddies approaching the continental slope from the deep ocean. In several open-ocean studies these energetic features of the ocean circulation have been observed and described during their propagation onto the continental shelf [*Lewis and Kirwan Jr.*, 1985; *Kirwan Jr. et al.*, 1988; *Vukovich and Waddel*, 1991; *Vidal et al.*, 1992; *Richardson et al.*, 1994; *Fratantoni et al.*, 1995; *Hamilton et al.*, 1999]. Studies that focus specifically on coastal eddies (the ones developed on the continental shelf) are much scarcer.

Mitchelson-Jacob and Sundby [2001] have observed coastal eddies through the analysis of satellite images on the continental shelf of Norway. They found that the size of these eddies depends on the width of the fjord, with a diameter between 20 km to 60 km. An anticyclonic eddy was sampled during a field campaign and followed by numerous drifters [*Mitchelson-Jacob and Sundby*, 2001; *Saetre*, 1999]. This anticyclonic eddy appeared to be a quasi-stationary feature [*Eide*, 1979], reaching 140 m depth. The wind direction, the depth of the near-surface layer and the presence of stratification have been identified as strong factors influencing the characteristics of these eddies. The strong currents in this region have been linked directly to the formation of these eddies.

Mesoscale anticyclonic eddies have been also investigated inside the Gulf of Alaska. These eddies are named according to the location of their generation: *Sitka Eddies* [*Tabata*, 1982], *Haida Eddies* [*Crawford and Whitney*, 1999] and *Yakutat Eddies* [*Ladd et al.*, 2005]. They are baroclinic structures with a diameter of 150-300 km. These eddies generally form in winter and detach from the continental margin in late winter and spring.

Haida Eddies usually form in the outflow of coastal waters [*Crawford*, 2002; *Di Lorenzo et al.*, 2005]. *Sitka* and *Yakutat Eddies* are believed to form in flow instabilities along the continental slope [*Melson et al.*, 1999].

Coastal cyclonic eddies have been also investigated further south along the British Columbia shelf. The presence of a quasi-stationary eddy, the *Juan de Fuca Eddy*, on the southern Vancouver Island shelf has been described in several studies [*Tully*, 1942; *Freeland and Denman*, 1982; *Denman and Freeland*, 1985; *Freeland and McIntosh*, 1989; *MacFadyen et al.*, 2008]. This eddy is a topographically confined eddy which develops off Cape Flattery in spring with a diameter of 80 km below 100 m depth.

Current separation from capes has been proposed as an explanation for eddy formation in many coastal flows behind capes or headlands [*Signell and Geyer*, 1991; *Doglioli et al.*, 2004; *Magaldi et al.*, 2010]. However, in the case of the buoyant flow around Cape Flattery, the Coriolis force does not tend to maintain the current close to the coast [*MacFadyen and Hickey*, 2010]. In fact, the eddy generation has been linked to two upwelling processes occurring in the area with the important contribution of tidal forcing in the initial eddy generation process [*Foreman et al.*, 2008; *MacFadyen and Hickey*, 2010].

In general, the dynamics and the role of mesoscale coastal eddies are very complex and different from one region to another. These eddies can translate away from their generation region with the mean flow [*Crawford et al.*, 2007; *Mitchelson-Jacob and Sundby*, 2001] or they can be quasi-stationary and linked to the topography [*Eide*, 1979; *Freeland and Denman*, 1982]. Other studies highlight the role of mesoscale eddies on coastal upwelling processes in idealized ecosystems [*Lathuilière et al.*, 2010] or in the Ligurian Sea [*Casella et al.*, 2011]. In either case, they have profound impacts on local mechanisms

of water transport, vertical mixing and circulation processes. They are often biologically rich regions because they can transport nutrient-rich coastal water off the coast to open ocean.

The Gulf of Lion (GoL) is particularly relevant for the study of coastal mesoscale structures. The GoL is located in the northwestern Mediterranean Sea and is characterized by a large continental margin (Figure 1). Its hydrodynamics is complex and highly variable [*Millot*, 1990]. The circulation is strongly influenced by the Northern Current (NC), which constitutes an effective dynamical barrier blocking coastal waters on the continental shelf [*Albérola et al.*, 1995; *Sammari et al.*, 1995; *Petrenko*, 2003]. Exchanges between the GoL and offshore waters are mainly induced by processes associated with the NC [*Conan and Millot*, 1995; *Flexas et al.*, 2002; *Petrenko et al.*, 2005].

In the eastern part of the GoL, south of Marseilles, *Allou et al.* [2010] have observed the presence of anticyclonic eddies between the NC and the coast using current meter data and surface currents measured by High Frequency (HF) radars. The eddies are of diameters 12 to 28 km and they are coherent down to a depth of 140 m. Baroclinic instability of the NC is a possible generation mechanism [*Flexas et al.*, 2002]. *Schaeffer et al.* [2011] have also observed anticyclonic eddies, with a diameter of 20-40 km, in the eastern part of the GoL with HF radars and numerical simulations. They have shown that their generation mechanism is related to the local wind conditions. After their generation, some of the eddies are advected by the NC towards the western part of the shelf.

The instability of the NC and its role on the advection of eddies has been also proposed to explain the presence of anticyclonic eddies on the Catalan continental shelf [*Rubio et al.*, 2005]. However *Rubio et al.* [2009a] rejected their previous hypothesis and suggested that

the process of flow separation due to a topographic barrier generates these eddies. A possible mechanism for the generation of the Catalan eddies is described by *Garreau et al.* [2011] in terms of release of potential energy from other eddies located in the GoL.

Through ADCP measurements and numerical simulations *Estournel et al.* [2003] showed a large anticyclonic circulation located in the northwestern part of the GoL. In this part of the GoL, a mesoscale anticyclonic circulation was first described by *Millot* [1979, 1982]. *Hu et al.* [2009, 2011a] showed the presence of a mesoscale eddy by a combined use of data from satellite observations, *in situ* measurements and numerical modeling. The eddies were baroclinic structures extending throughout the mixed layer (30 to 50 m), often elliptical in shape and about 20-30 km in diameter (elliptical diameter is defined as the mean of the minor and major axes). The generation process of the eddies mentioned by *Hu et al.* [2009, 2011a] required two conditions: a persistent and strong northwest wind and a strong stratification [*Hu et al.*, 2011b].

The LAgrangian Transport EXperiment (LATEX) project (2008-2011) is designed to study the mechanisms of formation of anticyclonic eddies and their influence on cross-shelf exchanges in the western part of the GoL. The dynamics of mesoscale eddies is particularly important in this part of the GoL since it represents a key region for regulating the outflow from the continental shelf [*Hu et al.*, 2011a; *Nencioli et al.*, 2011].

The aim of the present study is to analyze the dynamical characteristics and generation processes of such eddies during the summer of 2009. The methods used are described in Section 2. Results based on a combination of satellite and *in situ* oceanographic data, as well as numerical results are presented in Section 3. The general characteristics of the

observed eddies, their possible generation mechanisms and their behaviors are discussed in Section 4.

2. Methods

The LATEX strategy was based on a combined use of Eulerian and Lagrangian *in situ* measurements, satellite data and numerical modeling. The Latex09 campaign, conducted from August 24 to 28, 2009 on board the R/V Téthys II, was the second field experiment of the LATEX project.

2.1. Data

Identifying the center of an eddy is one of the greatest challenges in the eddy community. To characterize the observed eddy, this field campaign took advantage of various observational data.

The data collected during Latex09 came from satellite, ship-based and drifter observations. Satellite data include SeaWiFs chlorophyll concentration [mg m^{-3}] from the NASA's Goddard Space Flight Center (GSFC) and Sea Surface brilliance Temperature provided by Météo-France (referred to as SST_b). During the campaign, the data were sent to the R/V Téthys II to help tracking the mesoscale features in near real-time.

A VMBB-150 kHz ship-based Acoustic Doppler Current Profiler (ADCP) was used to measure current velocities (Figure 2). Following *Petrenko et al.* [2005], the instrument was configured for recording 1 minute ensemble averages, providing horizontal currents with a vertical resolution of 4 m from 11 to 247 m of depth. The software for ADCP raw data treatment is provided by the French Institut National des Sciences de l'Univers (INSU - CNRS) technical division. At each depth, the ADCP horizontal currents can be analyzed

in near real-time during the entire campaign using the method described by *Nencioli et al.* [2008]. A searching grid of 30×30 points corresponding to a 30×30 km square area was imposed within each transect. Each grid point was tested as a possible location, at that depth, for the center of the eddy. For each grid point, the components of the ADCP velocities from a transect were decomposed into radial and tangential components with respect to the reference frame centered at each point. The center, hereafter referred to as single-depth transect center, was estimated as the grid point for which the mean tangential velocity computed from the nearest ADCP records (black vectors - Figure 2) was maximum.

In the present paper, the analysis focuses on Transect 1 and three other transects that cross its center (Figure 2). Transect 2 is orthogonal to the coast (Figure 2b), Transect 3 is orthogonal to the continental slope (Figure 2c) and Transect 4 follows it (Figure 2d). The start and end times for each transect are reported in Table 1.

During the transect mapping, we also collected a total of 25 profiles at specific locations using a SeaBird SBE 19 CTD. We only show three of the CTD profiles, one inside the eddy (CTD_in, blue cross - Figure 5a), one at the edge (CTD_edge, red cross) and one outside the eddy (CTD_out, black cross), representing eddy center, eddy edge and outside conditions, respectively. Two satellite-tracked drifters, anchored at 15 m depth, were deployed within the eddy to track the fluid motion. Drifter positions were provided by the Argos system in quasi-real time. In addition, sea surface temperature, salinity and fluorescence were measured continuously at the surface by the ship's thermosalinometer SBE 21.

2.2. Ocean model

In addition to the *in situ* measurements, the eddy dynamics have been investigated using Symphonie, a 3-dimensional, primitive equation model, with a free sea surface, hybrid sigma coordinates, based on Boussinesq and hydrostatic approximations [*Marsaleix et al.*, 2006, 2008]. We use the upwind-type advection-diffusion scheme adapted by *Hu et al.* [2009] to improve the ability of the model to reproduce coastal mesoscale eddies in the western part of the GoL. In the present study, the model is implemented over the whole GoL with an horizontal resolution of 1 km $\times$ 1 km (Figure 1). The vertical discretization consists of 40-hybrid vertical levels. The vertical resolution varies from 1 m in the upper ocean to 40 m near the bottom.

This high resolution model is one-way nested to a coarse grid model (3 km $\times$ 3 km) covering a larger domain. The initial and open boundary conditions for the larger domain are provided by the Mediterranean Forecasting System (MFS) general circulation model [*Pinardi*, 2003] with a resolution of 1/8°. The atmospheric forcing is obtained from the 3-hr outputs of the meteorological model Aladin of Météo-France with a spatial resolution of 0.1°$\times$0.1°. The daily fresh water fluxes from the major rivers are taken into account. The readers are referred to *Hu et al.* [2011b] for more details about the model settings.

This model was run from 2001 to 2008 and the results were analyzed by *Hu et al.* [2011b]. In the present study it is run for 2009, with a restart from the previous simulation. The daily outputs of current velocity components, salinity, temperature and density are averaged over 24 hours of simulation, to filter out the diurnal cycle. We have verified that the 24-hours average is also effective in filtering out the inertial oscillations, that is of

~17.5 hours in the GoL. The remaining unfiltered inertial kinetic energy represents 1-5% of the total average kinetic energy.

In order to study the generation process with the same criteria used in the study of *Hu et al.* [2011a], we consider the wind as a strong and persistent northwesterly wind event when its amplitude is larger than, or equal to, 8 m s^{-1}, and its direction is between 270° and 360° for at least 75% of the time during the last three days. In order to investigate the variation of stratification, the potential energy anomaly ϕ is chosen as the indicator of the stability of the water column [*Hu et al.*, 2011a; *Burchard and Burchard*, 2008; *De Boer et al.*, 2008]. The value of ϕ decreases with the level of homogeneity through the water column. Values of ϕ reaching 20 J m^{-3} (100 J m^{-3}) indicate a weak (strong) stratification. An intermediate stratification is defined with a value ϕ around 60 J m^{-3}.

The utility program WATERS [*Doglioli et al.*, 2007] is used to objectively identify and follow the coherent eddy structures in our numerical simulations. This automatic detection of 3-dimensional eddy structures was first conducted with a high-resolution numerical model of the oceanic region around South Africa [*Doglioli et al.*, 2007]. More recently, WATERS has been used by *Rubio et al.* [2009b] to investigate mesoscale activity in the Benguela upwelling system and by *Dencausse et al.* [2010] to study the routes of Agulhas rings. In the South Atlantic Ocean, *Souza et al.* [2011] also tested the performances of WATERS in comparison with other automatic identification algorithms for the quantification and characterization of mesoscale eddies. In coastal waters, *Hu et al.* [2009, 2011b] successfully used WATERS to identify anticyclonic eddies in the GoL. The method is based on wavelet analysis of horizontal slices of modeled relative vorticity to extract coherent structures, providing a set of grid points and a center associated to each eddy. The

201 center of the modeled eddy is defined as the maximum in magnitude of relative vorticity.
202 For each eddy, tracking can be performed both backward and forward in time to find the
203 "birth" and the "death" of the eddy. At each time step, the eddy's diameter, D, is defined
204 as the average between the zonal (D^{EW}) and the meridional (D^{NS}) cords that intercept
205 each eddy center with both endpoints on the edge of the structure. This definition ac-
206 counts for stretched shapes. The analysis is repeated at each depth level (k) to diagnose
207 the vertical extent of the identified eddy. The vertical tracking ends at the level number
208 (i_z) before the eddy signal in relative vorticity becomes too weak to be detected. With
209 this method the reference diameter can be calculated as :

$$D = \frac{1}{i_z} \sum_{k=1}^{i_z} \frac{D_k^{EW} + D_k^{NS}}{2} \tag{1}$$

210

211 For stretched eddies, the variance made on the calculation of D with eq(1) is estimated
212 as:

$$D_{var} = \frac{1}{i_z} \sum_{k=1}^{i_z} \left(\frac{D_k^{EW} + D_k^{NS}}{2} - D \right)^2 \tag{2}$$

213

214 In the following, our results are written as $D \pm \sqrt{D_{var}}$.

3. Results

3.1. *In situ* experiment

215 An eddy was detected before the campaign from the analysis of the SST_b and SeaWiFs
216 chlorophyll-a surface concentration. On August 20, lower SST_b ($\Delta\ SST_b = 1.5$°C) and
217 lower chlorophyll-a concentration ($\Delta\ Chl_a = 0.4$ mg m^{-3}) within the eddy relative to the
218 surroundings, allowed for its identification. The eddy's center position was estimated to
219 be 3°30'E-42°36'N. At the beginning of the campaign, during Transect 1, we crossed the
220 whole eddy, passing through its satellite eddy center.

On the basis of ADCP velocities, the single-depth transect center for Transect 1 at 15 m depth *C1_15* was estimated to be at 3°33'E - 42°33'N (black cross - Figure 2a). Successively, we conducted a systematic mapping of the eddy by performing several transects passing through that position.

ADCP horizontal current velocity vectors at 15 m depth reveal a clockwise circulation associated with an anticyclonic eddy (Figure 2). We also detect a strong current with a southwestward direction at the southeastern part of the eddy, corresponding to the presence of the NC (Figures 2b,c).

Tangential velocity at 15 m depth and surface temperature measured during Transect 3 are shown in Figure 3 with respect to the distance from the single-depth transect center for Transect 3 at 15 m depth (*C3_15* - black cross - Figure 2c). Since Transect 3 did not pass directly through *C3_15*, the data are measured only up to a distance of 1.4 km from it. At this distance, the values of tangential velocities are not zero but close to zero. Then they increase linearly with radial distance to reach maximum values of about 0.4 m s^{-1} at roughly 9 km (15 km) for the northwestern (southeastern) part of the transect. These values show that the eddy is not symmetric. After reaching the maximum values, the tangential velocities slowly decrease as the radial distance further increases. The portion of the eddy characterized by a constant angular velocity corresponds to the portion of the eddy that rotates as a solid body (dashed line - Figure 3a). Thus the distance between the two maximum values of tangential velocities at the edges of the eddy, evaluated to be ~24 km (9 km +15 km), represents the diameter of the solid body rotation of the eddy.

The distribution of surface temperature from the thermosalinometer, with respect to radial distance from *C3_15*, shows warmer waters at the southeastern border of the eddy

(Figure 3b). The plot shows the presence of a strong temperature gradient (more than 1°C over a distance of ~3 km). This sudden temperature increase is located at 15 km from *C3_15*, and coincides with the maximum value of tangential velocity component, and hence the edge of the solid-body part of the eddy.

The vertical section of tangential velocity in Figure 4a, between 11 and 19 m depth, shows a typical eddy structure with two lobes of relatively high positive tangential velocities that extend on the two sides of the axis. A common feature for the tangential velocities at these depths is a quite rapid increase from the single-depth transect center for Transect 3 up to a distance of 10-15 km where they reach their maximum values. Between 19 and 31 m depth, tangential velocities never reach near zero values close to the single-depth transect center for Transect 3, as those at shallower depths do. This occurs because the deeper positions of the single-depth transect centers for Transect 3 tend to be further away from the transect (Figure 4b), indicating that the axis of the eddy is tilted. Below 31 m depth, velocities decay relatively rapidly with depth, so that the anticyclonic circulation associated with the eddy is limited to the upper 31 m. At deeper depths, the presence of the NC is most distinguishable between 3°42'E and 3°46'E with velocities around 0.2 m s^{-1}. The impact of the NC on the anticyclonic eddy is also obvious from the higher tangential velocities on its southeastern part at the surface.

In the preceding section we have only presented the analysis of Transect 3 at 15 m depth, since similar evaluations made for all the other transects gave similar results. Tangential velocities with respect to radial distance from the single-depth transect center have been analyzed for all the transects at three depths (11 m, 15 m, 19 m). These depths have been chosen because they are the shallowest bins available from the ADCP

and are within the studied eddy. The resulting estimations of the diameter and the position of the single-depth transect centers are summarized in Table 2. In the table we introduce two other center estimates. The depth-averaged transect centers are defined as the mean of the positions of the single-depth transect centers. The transect-averaged eddy center, hereafter named for simplification eddy center **C**, is defined as the mean of the positions of the depth-averaged transect centers. The estimated position of the eddy center corresponds to the depth-averaged transect center for Transect 1 (C1-Table 2).

Transects 3 and 4 are approximately meridional and zonal, respectively, and thus they are also roughly perpendicular (Figure 2). Therefore, in order to estimate the diameter from *in situ* data, we apply eq(1) where D_{EW} (D_{NS}) is the distance between the two maximum values of tangential velocities on Transect 3 (4) at the three reference depths (11 m, 15 m, 19 m). The diameter of the eddy is thereby estimated to be 22.7±1.2 km.

Another way to evaluate the vertical extension of the eddy comes from the analysis of the vertical profiles of temperature and fluorescence (Figure 5). The temperature profiles show values between 23.0°C and 23.6°C at the surface and a progressive decrease with depth to a value of 13.4°C at about 150 m depth (Figure 5b). A strong thermocline is observed between 8 and 18 m (20 and 35 m), at station CTD_out (CTD_in), outside (inside) the eddy. Indeed the anticyclonic eddy corresponds to a deepening of the thermocline. We also notice a weak value of fluorescence at the surface for all three profiles (Figure 5c). A fluorescence peak reaching 2.5 μg l^{-1} is visible at 50 m depth outside the eddy (station CTD_out); it decreases to less than 2 μg l^{-1} at the edge of the eddy (station CTD_edge). Only a faint maximum of 0.6 μg l^{-1} can be found at 70 m depth inside the eddy (station

289 CTD_in), deeper than the thermocline. This agrees with a reduced phytoplankton biomass
290 induced by the downwelling associated with anticyclonic eddies [*Siegel et al.*, 2011].

3.2. Modeling results

291 The study of the numerical model outputs with the wavelet analysis allows us to retrieve
292 information about the various mesoscale structures in the study area in 2009. Hereafter,
293 we adopt the terminology introduced by *Hu et al.* [2011b] who defined "long-life" eddies
294 as the ones which last for at least 15 days. We have thoroughly studied year 2009 and two
295 modeled "long-life" anticyclonic eddies are identified. The wavelet analysis shows that
296 the first "long-life" eddy (hereafter *A1*) is generated on June 28 and lasts until July 20,
297 while the second eddy is generated on August 16 and lasts until October 12. The latter is
298 considered to be analogous to the eddy sampled during Latex09 and described in Section
299 3.1, and hence is hereafter referred to as *A2-Latex09*.

300 First, we want to understand the generation mechanism of these two eddies. The
301 generation process of eddy *A1* starts with a strong northwesterly wind observed from
302 June 19 to 21. This strong wind, with an amplitude equal to 18 m s^{-1}, induces an Ekman
303 transport piling the water close to Cape Creus. Then a northward current along the
304 Roussillon coast starts on June 26. The closing of this Ekman southwestward drift and
305 coastal current jet generates the anticyclonic eddy. An intermediate stratification has also
306 been identified with an absolute value of potential energy anomaly more than 60 J m^{-3}.
307 These facts indicate that the generation process of the eddy *A1* corresponds to the one
308 described by *Hu et al.* [2011b] for all "long-life" eddies between 2001 and 2008.

309 On the other hand, the generation process of the second eddy, *A2-Latex09*, is different.
310 During a weak wind event (Figure 6a), we first observe the generation of a large-scale

anticyclonic circulation extending to all the western GoL on July 20 (Figure 6e). In the western part of the GoL, the positive sea surface height (Figure 6f) corresponds to an anticyclonic circulation extending south of Cape Creus. A meander of the NC approaches this large anticyclonic circulation, squeezing it and reinforcing the current at its southeastern edge. This occurs during a northwesterly wind event (Figure 6b) that started on August 6. It produces a localized upwelling south of Cape d'Agde but smaller than the one observed in the generation process proposed by *Hu et al.* [2011b]. During this generation process, the wind can be classified on August 27 as a strong northwesterly wind event (16 m s^{-1}) but not persistent since its occurrence during the last three days is less than 75%. A strong stratification has also been identified with an absolute value of potential energy anomaly more than 100 J m^{-3}. On August 16 the wavelet analysis identifies two anticyclonic eddies corresponding to the zonal separation of the anticyclonic area in two smaller areas (Figure 6g). Indeed the NC meander seems to push and squeeze the structure to the west. Then, as the presence of the coast blocks its progression, the structure becomes separated in two structures: one eddy on the shelf of the GoL (*A2-Latex09*) and one moving inside the Catalan Basin. On August 27, these structures are clearly distinct (Figure 6h). In the following, the eddy in the Catalan shelf is referred to as the *Catalan Eddy*.

In the next paragraphs, the characteristics of *A2-Latex09* on August 27 are presented for comparison with the *in-situ* data sampled at the same time (Table 1). The modeled *A2-Latex09* extends throughout the mixed layer until 37 m depth. The wavelet analysis identifies an eddy centered at 3°26'E-42°36'N with a diameter of 28.6±1.4 km. The position of the eddy's center is calculated as the mean of its positions between 1 and 37 m

depth with a vertical step of 4 m. This vertical step is chosen to be equal to the vertical resolution of the ADCP for a better comparison. The diameter of the eddy is obtained applying eq(1) and (2) to North/South and East/West transects across the modeled eddy with the same vertical resolution between the same depth interval.

Moreover the model has been also useful to examine the post generation mechanism of *A2-Latex09*. Indeed on August 31, *A2-Latex09* encounters Cape Creus. Following this event, a transient anticyclonic structure is generated downstream the cape on September 3, detaching from *A2-Latex09*. A 3D view of potential vorticity (Figure 7) in the domain gives a good visualization of the phenomenon. In order to quantify the transfer, a balance of mass has been computed from the model results between August 30 and September 3.

The transient structure represents ~33% of the *A2-Latex09*'s mass. The loss of mass of the eddy *A2-Latex09* is estimated to be ~41%. As a result, 8% of the mass is dispersed during this separation. The gain expected on the mass of the *Catalan Eddy* can not be estimated properly since the latter is too close to the model domain boundary.

A 2D view of the relative vorticity (Figure 8a) shows the presence of the transient anticyclonic structure between *A2-Latex09* and the *Catalan Eddy*. The dynamics simulated by the model is supported by the trajectories of two Lagrangian drifters, released during the Latex09 campaign, from August 26 to September 12 (Figure 8b). On August 26, drifter No. 83631 (blue line) was deployed near the eddy center **C** and drifter No. 83632 (purple line) near the western outer edge of the eddy. Drifter No. 83631 made one full loop around the eddy in 81 hours. Its trajectory stopped looping around the eddy on September 2 and then drifted northward. Drifter No. 83632 started to loop around the eddy but, on August 30, it began to drift southward moving away from it. Checking the

rotation period of this buoy to ascertain the nature of this feature, we found a rotation period of 39 hours, corresponding approximately to half the rotation period of *A2-Latex09*. This rotation does not correspond to an inertial oscillation, which has a typical period of ~17.5 hours in the GoL. This fact confirms the hypothesis that the drifter is trapped in the transient structure. On September 6, Drifter No. 83632 got trapped in the *Catalan Eddy* located at 3°11'E-41°35'N.

4. Discussion and Concluding remarks

The generation and characteristics of a coastal anticyclonic eddy detected in the western part of the GoL have been studied from a combination of *in situ* measurements and numerical modeling from the end of August 2009 to the middle of October 2009.

On the basis of *in situ* measurements, the anticyclonic eddy is centered at 3°34'E-42°33'N and is characterized by a diameter of 22.7±1.2 km, reaching a maximal depth of 31 m. The observed anticyclonic eddy is well reproduced by the model as shown by the numerical relative vorticity field on September 3 (Figure 8a). The major characteristics of this modeled eddy agree with the observations, although its horizontal dimensions are slightly larger than the observed ones. The diameter of the simulated eddy is 28.6±1.4 km. This eddy is approximately situated at the same location as the measured one, slightly more northwestward (3°26'E-42°36'N).

To characterize the dynamics of the eddy, we computed the local Rossby number ($R_o = \frac{V_{max}}{R_{max} f}$) and the the Rossby radius of deformation ($R_d = \frac{\sqrt{g' H'}}{f}$). V_{max} is calculated as the mean of the maximum tangential velocities on Transects 3 and 4 at the three reference depths. R_{max} is calculated as half of the reference diameter D, defined in eq(1). With V_{max} equal to 0.35 m s^{-1} and R_{max} about 13.5 km, the resulting local Rossby number of

the eddy is 0.26. To compute R_d, the reduced gravity was calculated as $g' = \frac{\rho_2 - \rho_1}{\rho_2} g$, with $\rho_2 = 1029.04$ kg m^{-3}, the mean density below the mixed layer, and $\rho_1 = 1025.75$ kg m^{-3}, the mean density within the mixed layer. The mixed layer depth was 10.9 m. The resulting R_d is 5.9 km, which is smaller than the eddy reference radius R_{max}. Since $R_{max} > R_d$, we can objectively classify the eddy as a mesoscale structure. Since the local Rossby number is not small, its dynamics can not be approximated by quasi-geostrophic theory.

We can compare our results with the data gathered during the experiment Latex08 in the same area [*Hu et al.*, 2011a] conducted from September 1 to 5, 2008. Although the generation process is different, these two coastal anticyclonic eddies have similar characteristics in terms of position, extension and dynamical characteristics. This fact shows the important influence of coast and bathymetry on the physical characteristics of these mesoscale eddies.

Hu et al. [2011a] emphasized that the 2008 eddy interacts with the Northern Current at the end of the Latex08 campaign, leading to its deformation and maybe to its death. In our case, the presence and role of the Northern Current is much clearer (Figures 2b,c). The NC has first created the eddy and then it affected it, reinforcing the current at its southeastern part. This intensification could explain the asymmetric shape of the eddy.

Regarding the possible mechanisms for the formation of these anticyclonic eddies in the literature, a few processes of generation have been listed in the introduction. The numerical study of eddy generation in the western part of the GoL by *Hu et al.* [2011b] shows that these eddies need two conditions to be generated: a persistent and strong northwest wind and a strong stratification. This mechanism of generation has been identified in our analysis. Indeed, the process of generation of the first modeled anticyclonic eddy *A1* cor-

responds to *Hu et al.* [2011b]'s process with the two conditions described above. A strong northwesterly wind is observed from June 19 to 21 and an intermediate stratification is noted at the end of June with an absolute value of potential energy anomaly greater than 60 J m^{-3}.

Instead, for anticyclonic eddy *A2-Latex09*, we propose a new process of generation, associated with the NC. This new mechanism starts with the generation of an anticyclonic circulation extending over a large part of the coastal area (Figure 6e). The generation of this anticyclonic circulation, precursor to the eddy, is not analyzed in this study but it could have been generated by the mechanism proposed by *Hu et al.* [2011b]. Interaction with a meander of the Northern Current and the presence of the coast induces the latitudinal separation of this anticyclonic circulation into two eddies, the northern one in the GoL and the southern one on the Catalan shelf. To our knowledge, this generation process has not been proposed before. Indeed the combined analysis of *Rubio et al.* [2005, 2009a] suggests that Catalan eddies are generated downstream of Cape Creus as a result of a flow separation triggered by an intense northwest wind event in the GoL. While *Garreau et al.* [2011] indicate that GoL eddies flow southward creating Catalan eddies after a burst of southeasterlies and northerlies. The authors conclude that the death of GoL eddies is clearly linked to the birth of strong Catalan eddies. In our case, the detachment of a part of the eddy does not lead to the death of *A2-Latex09*. The formation of this transient structure comes from the encounter of the *A2-Latex09* with Cape Creus. The generation of this transient structure causes a loss of mass and vorticity for *A2-Latex09*. In the *in-situ* measurements, a small structure is detected in the same spatial area and at the same time (Figure 8b) as the one given by the model (Figure 8a). When drifter No. 83632 starts

to loop outside the eddy (Figure 8b), drifting toward the south, its rotation period (39 hours) eliminates the occurrence of an inertial oscillation. After ~6 days this drifter is caught by the *Catalan Eddy* located at 3°11'E-41°35'N. The generation of the transient structure moving from *A2-Latex09* toward the *Catalan Eddy* in the model results can explain the trajectories of these drifters. From the *in-situ* experiment it is clear that the generation of this structure leads directly to a transfer of mass from the eddy of the GoL to the eddy of the Catalan shelf.

This study gives a more complete and consistent picture of the GoL coastal eddy dynamics. A full 3D analysis from numerical simulation will be made with the objective of better understanding the remaining open questions about the generation of the anticyclonic circulation, first step of the proposed new generation process. Besides, this numerical modeling work would be useful to explore the coupled physical and biogeochemical dynamics at mesoscale and the role of mesoscale eddies in the transfers between the GoL coastal zone and the neighboring coastal regions.

Acknowledgments. The LATEX project is supported by the programs LEFE/IDAO and LEFE/CYBER of the INSU-Institut National des Sciences de l'Univers and by the Region PACA-Provence Alpes Côte d'Azur. The meteorological data were kindly supplied by Météo-France. We acknowledge the MFS program for OGCM outputs. We are warmly grateful to the crews of the R/V Téthys II for their assistance. We thank Z. Y. Hu for providing the last configuration of the model. The authors want to thank J. Bouffard and C. Yohia for precious comments and useful discussions. Marion Kersalé is financed by a MENRT Ph.D. grant.

References

Albérola, C., C. Millot, and J. Font (1995), On the seasonal and mesoscale variabilities of the Northern Current during the PRIMO-0 experiment in the western Mediterranean Sea, *Oceanol. Acta*, *18*(2), 163–192.

Allou, A., P. Forget, and J. L. Devenon (2010), Submesoscale vortex strucures at the entrance of the Gulf of Lions in the Northwestern Mediterranean Sea, *Cont. Shelf Res.*, *30*, 724–732, doi:10.1016/j.csr.2010.01.006.

Burchard, H., and R. Burchard (2008), A dynamic equation for the potential energy anomaly for analysing mixing and stratification in estuaries and coastal seas, *Estuarine, Coastal Shelf Science*, *77*(4), 679–687, doi:10.1016/j.ecss.2007.10.025.

Casella, E., A. Molcard, and A. Provenzale (2011), Mesoscale vortices in the Ligurian Sea and their effect on coastal upwelling processes, *J. Mar. Sys.*, *88*(1), 12–19, doi: 10.1016/j.jmarsys.2011.02.019.

Conan, P., and C. Millot (1995), Variability of the Northern Current off Marseilles, western Mediterranean Sea, from February to June 1992, *Oceanol. Acta*, *18*(2), 193–205.

Crawford, W. R. (2002), Physical characteristics of Haida Eddies, *Journal of Oceanography*, *58*(5), 703–713, doi:10.1023/A:1022898424333.

Crawford, W. R., and F. A. Whitney (1999), Mesoscale eddy aswirl with data in Gulf of Alaska Ocean, *Eos, Trans. AGU*, *80*(33), 365–670.

Crawford, W. R., P. J. Brickley, and A. C. Thomas (2007), Mesoscale eddies dominate surface phytoplankton in northern Gulf of Alaska, *Prog. Oceanogr.*, *75*, 287–303, doi: 10.1016/j.pocean.2007.08.016.

De Boer, G. J., J. D. Pietrzak, and J. C. Winterwerp (2008), Using the potential energy anomaly equation to investigate tidal straining and advection of stratification in a region of freshwater influence, *Ocean Model.*, *22*, 1–11.

Dencausse, G. J., M. Arhan, and S. Speich (2010), Routes of agulhas rings in the south eastern cape basin, *Deep-Sea Res. I*, *57*, 1406–1421, doi:10.1016/j.dsr.2010.07.008.

Denman, K. L., and H. J. Freeland (1985), Correlation scales, objective mapping and a statistical test of geostrophy over the continental shelf, *J. Mar. Res.*, *43*(3), 517–539, doi:10.1357/002224085788440402.

Di Lorenzo, E., M. G. G. Foreman, and W. R. Crawford (2005), Modelling the generation of Haida Eddies, *Deep-Sea Res. II*, *52*, 853–873, doi:10.1016/j.dsr2.2005.02.007.

Doglioli, A. M., A. Griffa, and M. G. Magaldi (2004), Numerical study of a coastal current on a steep slope in presence of a cape: The case of the Promontorio di Portofino, *J. Geophys. Res.*, *109*, C12033, doi:10.1029/2004JC002422.

Doglioli, A. M., B. Blanke, S. Speich, and G. Lapeyre (2007), Tracking coherent structures in a regional ocean model with wavelet analysis: application to Cape Basin Eddies, *J. Geophys. Res.*, *112*, C05043, doi:10.1029/2006JC003952.

Eide, L. I. (1979), Evidence of a topographically trapped vortex on the Norwegian continental shelf, *Deep-Sea Res. I*, *26*(6), 601–621, doi:10.1016/0198-0149(79)90036-0.

Estournel, C., X. Durrieu de Madron, P. Marsaleix, F. Auclair, C. Julliand, and R. Vehil (2003), Observation and modeling of the winter coastal oceanic circulation in the Gulf of Lion under wind conditions influenced by the continental orography (FETCH experiment), *J. Geophys. Res.*, *108*(C3), 8059, doi:10.1029/2001JC000825.

Flexas, M. M., X. Durrieu de Madron, M. A. Garcia, M. Canals, and P. Arnau (2002), Flow variability in the Gulf of Lions during the MATER HFF experiment (March-May 1997), *J. Mar. Sys.*, *33-34*, 197–214, doi:DOI: 10.1016/S0924-7963(02)00059-3.

Foreman, M. G. G., W. Callendar, A. MacFadyen, B. M. Hickey, R. E. Thomson, and E. Di Lorenzo (2008), Modeling the generation of the juan de fuca eddy, *J. Geophys. Res.*, *113*(C03006), doi:10.1029/2006JC004082.

Fratantoni, D. M., W. E. Johns, and T. L. Townsend (1995), Rings of the North Brazil Currents: their structure and behavior inferred from observations and a numerical simulation, *J. Geophys. Res.*, *100*(C6), 10.633–10.654, doi:10.1029/95JC00925.

Freeland, H. J., and K. L. Denman (1982), A topographically controlled upwelling center off southern Vancouver Island, *J. Mar. Sys.*, *40*(4), 1069–1093.

Freeland, H. J., and P. McIntosh (1989), The vorticity balance on the southern British Columbia continental shelf, *Atmos.-Ocean*, *27*(4), 643–657.

Garreau, P., V. Garnier, and A. Schaeffer (2011), Eddy resolving modelling of the Gulf of Lions ans Catalan Sea, *Ocean Dynam.*, *61*, 991–1003, doi:10.007/s10236-011-0399-2.

Hamilton, P., G. S. Fargion, and D. C. Biggs (1999), Loop Current eddy paths in the western Gulf of Mexico, *J. Phys. Oceanogr.*, *29*(6), 1180–1207, doi:10.1175/1520-0485(1999)029¡1180:LCEPIT¿2.0.CO;2.

Hu, Z. Y., A. A. Doglioli, A. M. Petrenko, P. Marsaleix, and I. Dekeyser (2009), Numerical simulations of eddies in the Gulf of Lion, *Ocean Model.*, *28*(4), 203 – 208, doi:10.1016/j.ocemod.2009.02.004.

Hu, Z. Y., A. A. Petrenko, A. M. Doglioli, and I. Dekeyser (2011a), Study of mesoscale anticyclonic eddy in the western part of the Gulf of Lion, *J. Mar. Sys.*, *88*, 3–11, doi:

513 10.1016/j.jmarsys.2011.02.008.

514 Hu, Z. Y., A. A. Petrenko, A. M. Doglioli, and I. Dekeyser (2011b), Numerical study of
515 eddy generation in the western part of the Gulf of Lion, *J. Geophys. Res.*, *116*, C12030,
516 doi:10.1029/2011JC007074.

517 Kirwan Jr., A. D., J. K. Lewis, A. W. Indest, P. Reinersman, and I. Quintero (1988),
518 Observed and Simulated Kinematic Properties of Loop Current Rings, *J. Geophys. Res.*,
519 *93*(C2), 1189–1198, doi:10.1029/JC093iC02p01189.

520 Ladd, C. M., N. B. Kachel, C. W. Mordy, and P. J. Stabeno (2005), Observations from
521 a Yakutat eddy in the northern Gulf of Alaska, *J. Geophys. Res.*, *110*(C03003), doi:
522 10.1029/2004JC002710.

523 Lathuilière, C., V. Echevin, M. Lévy, and G. Madec (2010), On the role of the mesoscale
524 circulation on an idealized coastal upwelling ecosystem, *J. Geophys. Res.*, *115*, C09018,
525 doi:10.1029/2009JC005827.

526 Lewis, J. K., and A. D. Kirwan Jr. (1985), Some observations of ring topography and
527 ring-ring interactions in the Gulf of Mexico, *J. Geophys. Res.*, *90*(C5), 9017–9028, doi:
528 10.1029/JC090iC05p09017.

529 MacFadyen, A., and B. M. Hickey (2010), Generation and evolution of a topographically
530 linked, mesoscale eddy under steady and variable wind-forcing, *Cont. Shelf Res.*, *30*(13),
531 1387–1402, doi:10.1016/j.csr.2010.04.001.

532 MacFadyen, A., B. M. Hickey, and W. P. Cochlan (2008), Influences of the Juan de Fuca
533 Eddy on circulation, nutrients, and phytoplankton production in the northern California
534 Current System, *J. Geophys. Res.*, *113*(C08008), doi:10.1029/2007JC004412.

Magaldi, M., T. Özgökmen, A. Griffa, and M. Rixen (2010), On the response of a turbulent coastal buoyant current to wind events: the case of the Western Adriatic Current, *Ocean Dynam.*, *60*, 93–122, doi:10.1007/s10236-009-0247-9.

Marsaleix, P., F. Auclair, and C. Estournel (2006), Considerations on Open Boundary Conditions for Regional and Coastal Ocean Models, *J. Atmos. Ocean. Technol.*, *23*, 1604–1613, doi:10.1175/JTECH1930.1.

Marsaleix, P., F. Auclair, J. Floor, M. Herrmann, C. Estournel, I. Pairaud, and C. Ulses (2008), Energy conservation issues in sigma-coordinate free-surface ocean models, *Ocean Model.*, *20*, 61–89, doi:10.1016/j.ocemod.2007.07.005.

Melson, A., S. D. Meyers, H. E. Hurlburt, E. J. Metzger, and J. J. O'Brien (1999), ENSO effects on Gulf of Alaska eddies, *Earth Interactions 3*, *003*, doi:10.1175/1087-3562.

Millot, C. (1979), Wind induced upwellings in the Gulf of Lions, *Oceanol. Acta*, *2*, 261–274.

Millot, C. (1982), *Analysis of upwelling in the Gulf of Lions - Hydrodynamics of semi-enclosed seas: Proceedings of the 13th International Liège Colloquium on Ocean Hydro-dynamics.*, vol. 34, 143-153 pp., Elsevier Oceanogr. Ser., Amsterdam, The Netherlands.

Millot, C. (1990), The Gulf of Lions' hydrodynamics, *Cont. Shelf Res.*, *10*, 885–894, doi:10.1016/0278-4343(90)90065-T.

Mitchelson-Jacob, G., and S. Sundby (2001), Eddies of Vestfjorden, Norway, *Cont. Shelf Res.*, *21*(16-17), 1901–1918, doi:10.1016/S0278-4343(01)00030-9.

Nencioli, F., V. S. Kuwahara, T. D. Dickey, Y. M. Rii, and R. R. Bidigare (2008), Physical dynamics and biological implications of a mesoscale eddy in the lee of Hawai'i : Cyclone Opal observations during E-FLUX III, *Deep-Sea Res. II*, *55*(10-13), 1252–1274, doi:

10.1016/j.dsr2.2008.02.003.

Nencioli, F., F. d'Ovidio, A. M. Doglioli, and A. A. Petrenko (2011), Surface coastal circulation patterns by in-situ detection of Lagrangian coherent structures, *Geophys. Res. Lett.*, *38*(L17604), doi:10.1029/2011GL048815.

Petrenko, A. A. (2003), Variability of circulation features in the Gulf of Lion NW Mediterranean Sea. Importance of inertial currents, *Oceanol. Acta*, *26*, 323–338.

Petrenko, A. A., Y. Leredde, and P. Marsaleix (2005), Circulation in a stratified and wind-forced Gulf of Lions, NW Mediterranean Sea: in situ and modeling data, *Cont. Shelf Res.*, *25*, 7–27, doi:10.1016/j.csr.2004.09.004.

Pinardi, N. (2003), The Mediterranean ocean forcasting system : first phase of implementation (1998-2001), *Ann. Geophys.*, *21*, 3–20, doi:10.5194/angeo-21-3-2003.

Richardson, P. L., G. E. Hufford, and R. I. Limeburner (1994), North Brazil Current retroflection eddies, *J. Geophys. Res.*, *99*(C3), 5081–5093, doi:doi:10.1029/93JC03486.

Rubio, A., P. Arnau, M. Espino, M. Flexas, G. Jordà, J. Salat, J. Puigdefàbregas, and A. S.-Arcilla (2005), A field study of the behaviour of an anticyclonic eddy on the Catalan continental shelf (NW Mediterranean), *Prog. Oceanogr.*, *66*(2-4), 142–156, doi:10.1016/j.pocean.2004.07.012.

Rubio, A., B. Barnier, G. Jordà, M. Espino, and P. Marsaleix (2009a), Origin and dynamics of mesoscale eddies int he Catalan Sea (NW Mediterranean): Insight from a numerical model study, *J. Geophys. Res.*, *114*(C06009), 1–17, doi:10.1029/2007JC004245.

Rubio, A., B. Blanke, S. Speich, N. Grima, and C. Roy (2009b), Mesoscale eddy activity in the southern Benguela upwelling system from satellite altimetry and model data, *Prog. Oceanogr.*, *83*(1-4), 288–295, doi:10.1016/j.pocean.2009.07.029.

Saetre, R. (1999), Features of the central Norwegian shelf, *Cont. Shelf Res.*, *19*(14), 1809–1831, doi:10.1016/S0278-4343(99)00041-2.

Sammari, C., C. Millot, and L. Prieur (1995), Aspects of the seasonal and mesoscale variabilities of the Northern Current inferred from the PROLIG-2 and PROS-6 experiments, *Deep-Sea Res. I*, *42*(6), 893–917, doi:10.1016/0967-0637(95)00031-Z.

Schaeffer, A., A. Molcard, P. Forget, P. Fraunié, and P. Garreau (2011), Generation mechanisms for mesoscale eddies in the Gulf of Lions : radar observation and modeling, *Ocean Dynam.*, *61*, 1587–1609, doi:10.1007/s10236-011-0482-8.

Siegel, D. A., P. Peterson, D. J. McGillicuddy, S. Maritorena, and N. B. Nelson (2011), Biooptical footprints created by mesoscale eddies in the Sargasso Sea, *Geophys. Res. Lett.*, *38*(L13608), doi:doi:10.1029/2011GL047660.

Signell, R. P., and W. R. Geyer (1991), Transient eddy Formation Around Headlands, *J. Geophys. Res.*, *96*(C2), 2561–2575, doi:10.1029/90JC02029.

Souza, J. M. A. C., C. de Boyer Montégut, and P. Y. Le Traon (2011), Comparison between three implementations of automatic identification algorithms for the quantification and characterization of mesoscale eddies in the South Atlantic Ocean, *Ocean Sc.*, *7*, 317–334, doi:10.5194/os-7-317-2011.

Tabata, S. (1982), The anticyclonic baroclinic eddy off Sitka, Alaska, in the northeast Pacific Ocean, *J. Phys. Oceanogr.*, *12*, 1260–1282, doi:10.1175/1520-0485(1982)012<1260:TABEOS>2.0.CO;2.

Tully, J. (1942), Surface non-tidal currents in the approaches to Juan de Fuca Strait, *J. Fish. Res. Board Can.*, *5b*(4), 398–409, doi:10.1139/f40-041.

Vidal, V. M. V., F. V. Vidal, and J. M. Perez-Molero (1992), Collision of a Loop Current anticyclonic ring against the continental slope of the western Gulf of Mexico, *J. Geophys. Res.*, *97*(C2), 2155–2172, doi:10.1029/91JC00486.

Vukovich, F. M., and E. Waddel (1991), Interaction of a warm ring with the western slope in the Gulf of Mexico, *J. Phys. Oceanogr.*, *21*(7), 1062–1074.

Table 1. Start and end dates of the transects.

Transect	Start		End	
	Day	Hour (GMT)	Day	Hour (GMT)
1	Aug. 25	01h38	Aug. 25	04h48
2	Aug. 25	18h27	Aug. 25	23h39
3	Aug. 26	21h24	Aug. 27	01h16
4	Aug. 27	21h31	Aug. 28	03h54

Table 2. Summary of the calculation of the position of the center of the eddy for each transect. The along transect diameter at the depth given in column 2 is provided in column 3.

Transect	Depth (m)	Diameter (km)	Single-depth transect center	Depth-averaged transect center	Transect-averaged eddy center
1	-11	30	*C1_11*: 3°33'E - 42°33'N	C1: 3°34'E - 42°33'N	**C**: 3°34'E - 42°33'N
	-15	33	*C1_15*: 3°33'E - 42°33'N		
	-19	35	*C1_19*: 3°35'E - 42°33'N		
2	-11	30	*C2_11*: 3°35'E - 42°30'N	C2: 3°34'E - 42°31'N	
	-15	29	*C2_15*: 3°33'E - 42°31'N		
	-19	28	*C2_19*: 3°33'E - 42°32'N		
3	-11	24	*C3_11*: 3°35'E - 42°30'N	C3: 3°36'E - 42°32'N	
	-15	24	*C3_15*: 3°35'E - 42°33'N		
	-19	26	*C3_19*: 3°36'E - 42°34'N		
4	-11	24	*C4_11*: 3°33'E - 42°33'N	C4: 3°35'E - 42°34'N	
	-15	22	*C4_15*: 3°34'E - 42°34'N		
	-19	16	*C4_19*: 3°37'E - 42°34'N		

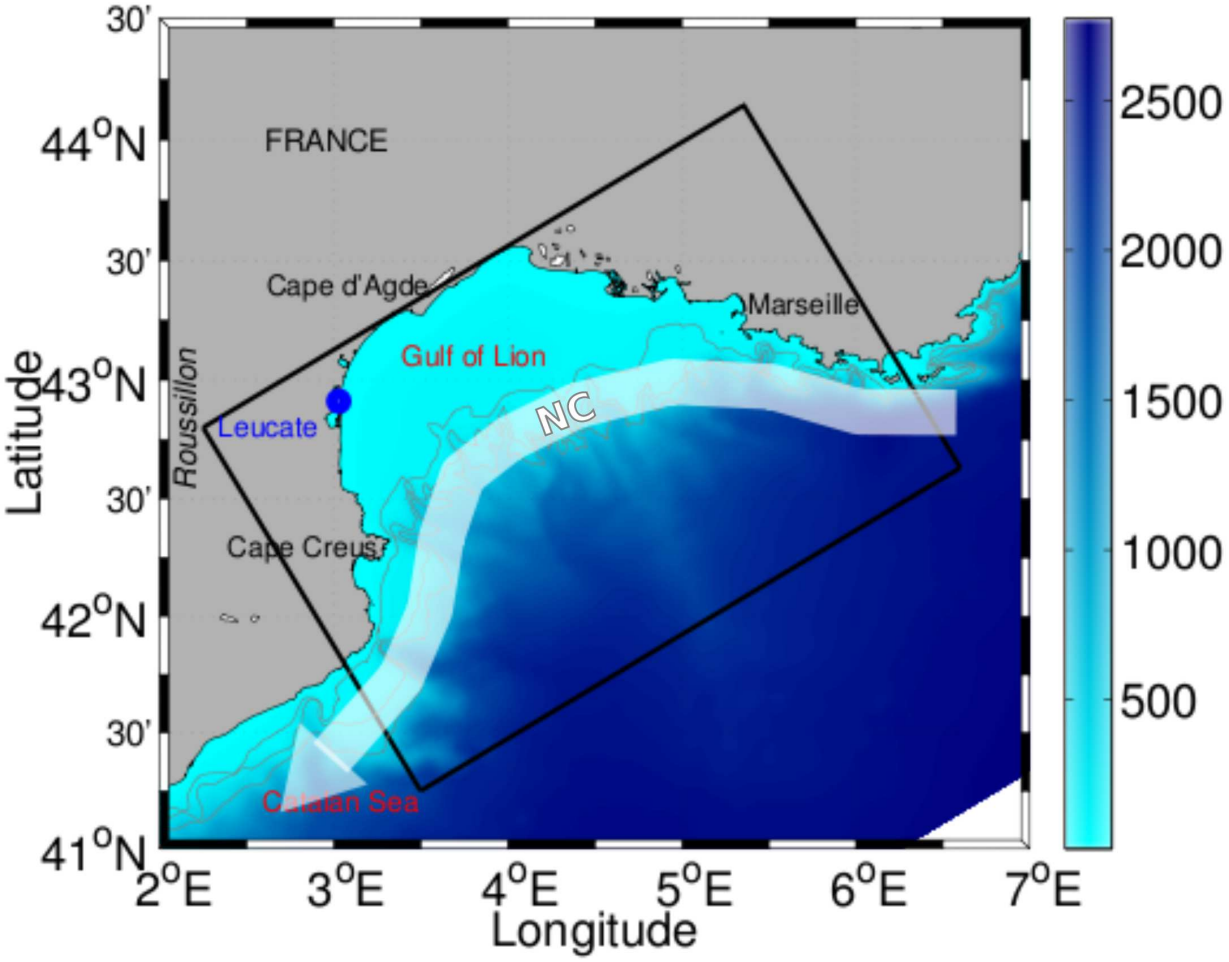

Figure 1. Model domain. The rectangle represents the model domain of 1 km × 1 km resolution. Shaded color represents the bathymetry [m]. Isobaths at 100, 200 and 500 m are plotted with thin lines. The white arrow shows the mean position of the Northern Current (NC).

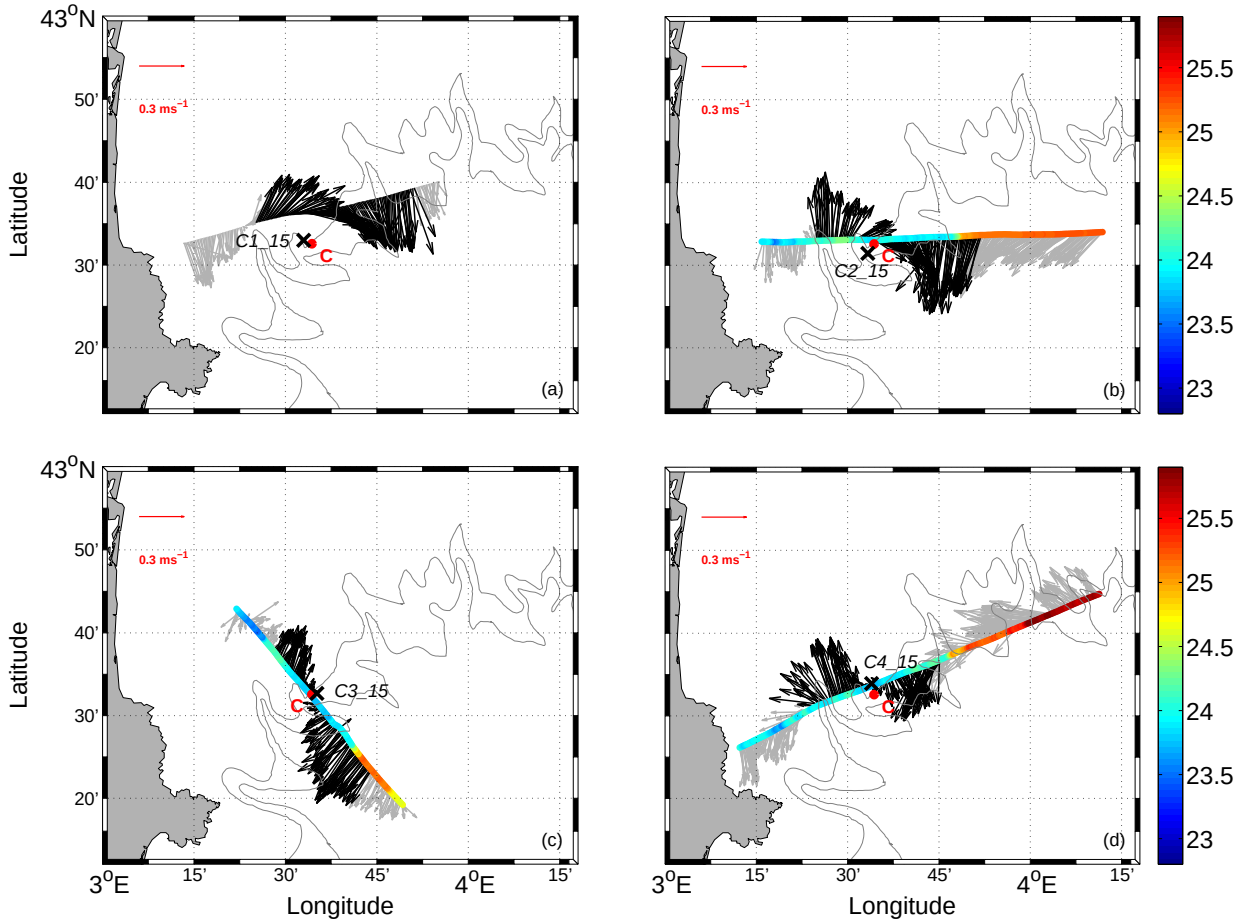

Figure 2. ADCP current vectors at 15m depth for Transect 1 (a), Transect 2 (b), Transect 3 (c) and Transect 4 (d). The colors on the transect represent the surface temperature data (°C) acquired along the trajectory. For each transect, the single-depth transect center at 15 m depth (black cross) is defined as the point for which the mean tangential velocity computed from the velocity vectors in black is maximum. The red dot corresponds to the eddy center.

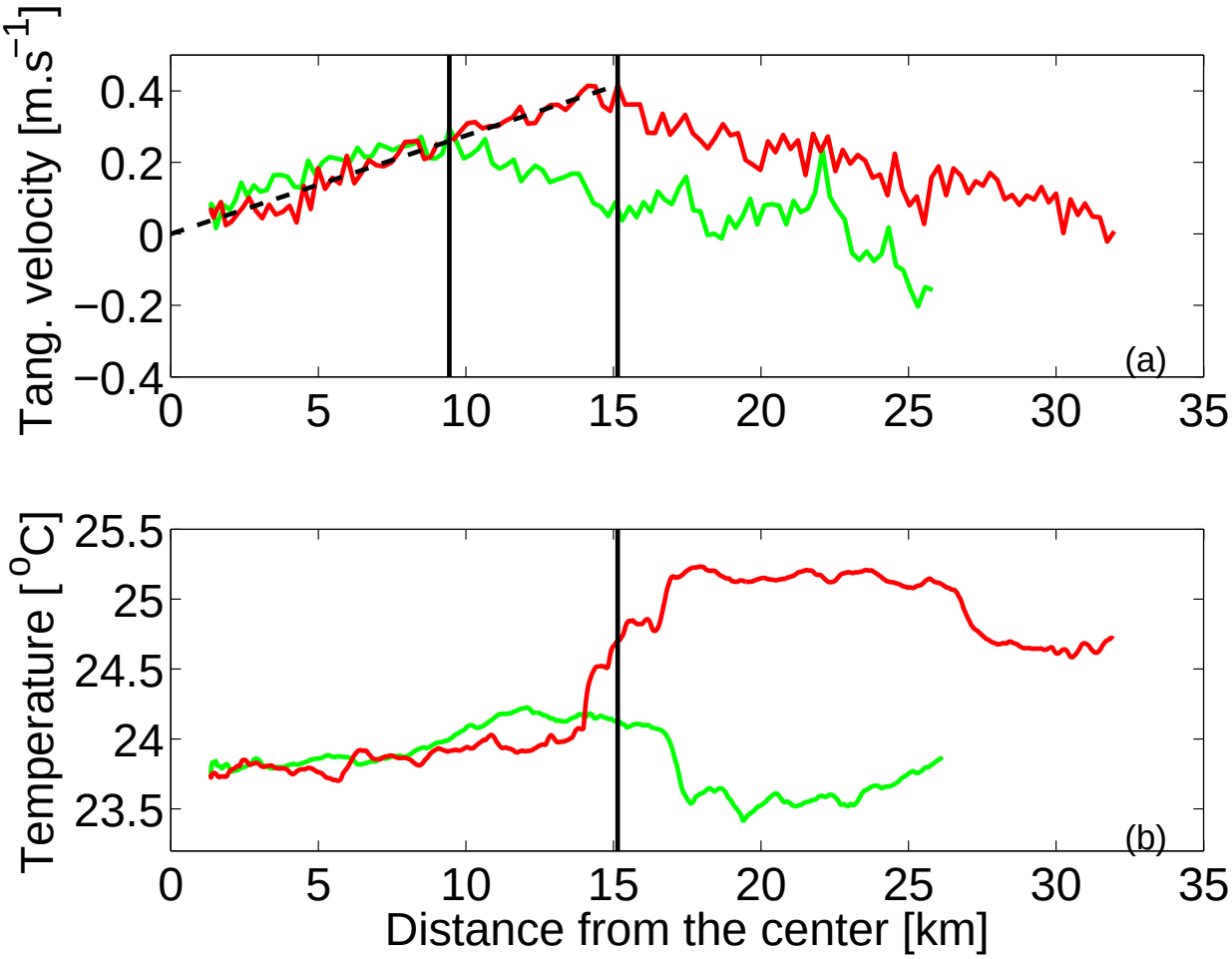

Figure 3. Distribution of tangential velocities at 15 m depth (a) and temperature at the surface (b) with respect to radial distance from *C3_15*. The green line corresponds to the data collected before crossing the center (hence northwest of the center *C3_15* for Transect 3) and the red line corresponds to the data collected after the center (southeast of it). Black lines represent the distance from *C3_15* where the maximum values of tangential velocities are reached. The black dashed line shows the linear increase of the tangential velocities in the case of a theoretical solid body rotation.

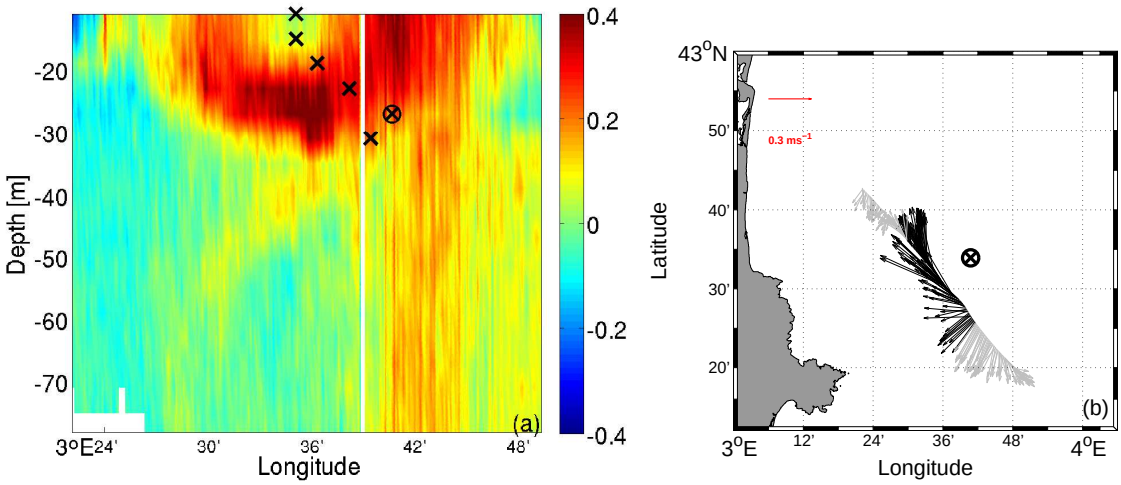

Figure 4. (a) Vertical section (depth versus longitude) of the tangential component (clockwise, positive) of the horizontal currents [m s^{-1}] for Transect 3. White pixels represent no data. ADCP current vectors at 27 m depth (b) for Transect 3. The black cross represent the single-depth transect center. The black circle represents the single-depth transect center at 27 m depth, common to figures a and b.

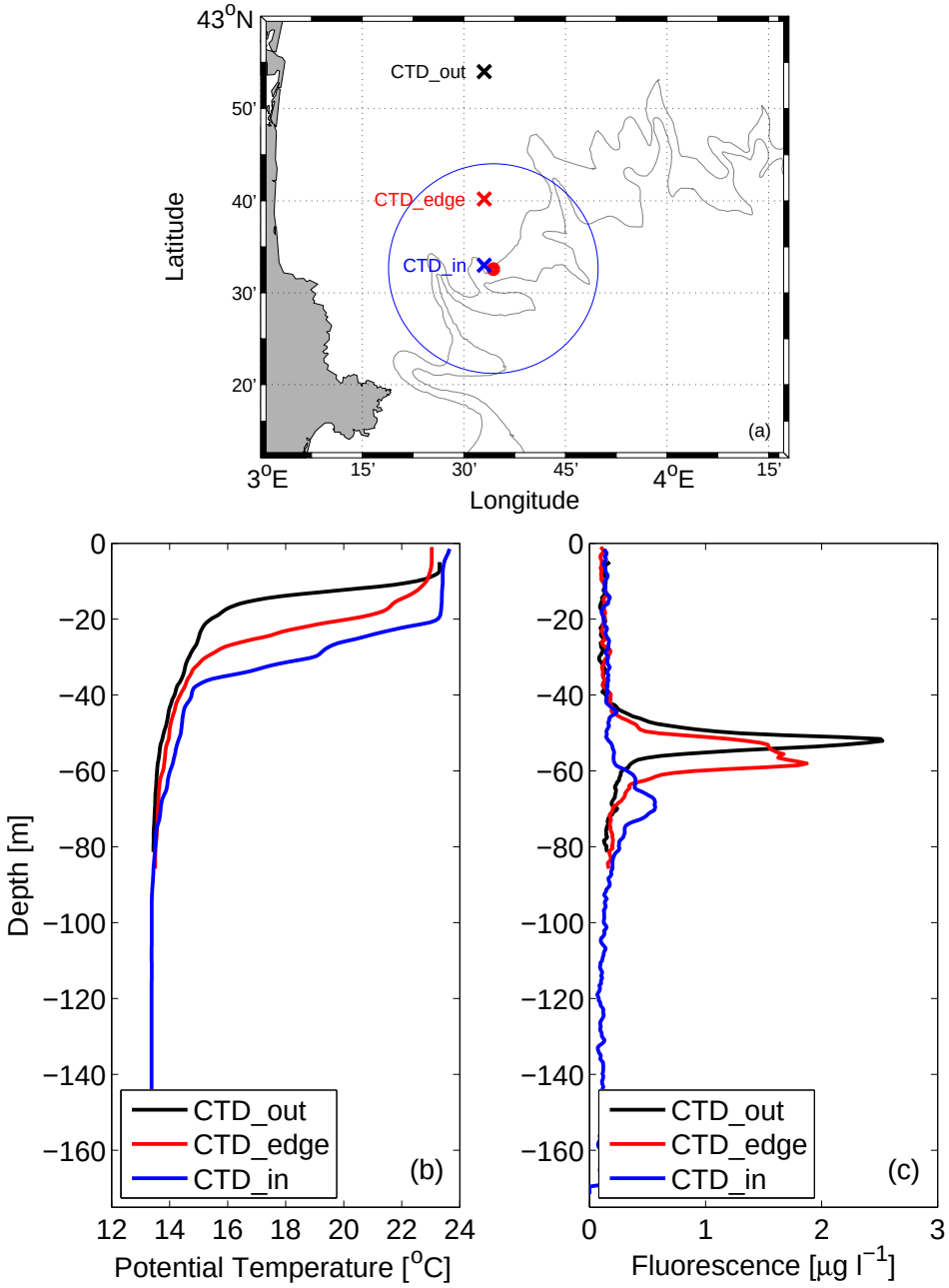

Figure 5. (a) The three crosses represent the positions of the CTD stations (CTD_in, CTD_edge, CTD_out). The blue circle is centered at the eddy center **C** (red dot) with a radius equal to the one estimated for the eddy. Vertical profiles of potential temperature (b) and fluorescence (c) at three CTD stations on August 26 (CTD_out: Outside part of the eddy located to the north; CTD_edge: Northern edge of the eddy; CTD_in: Inside part of the eddy).

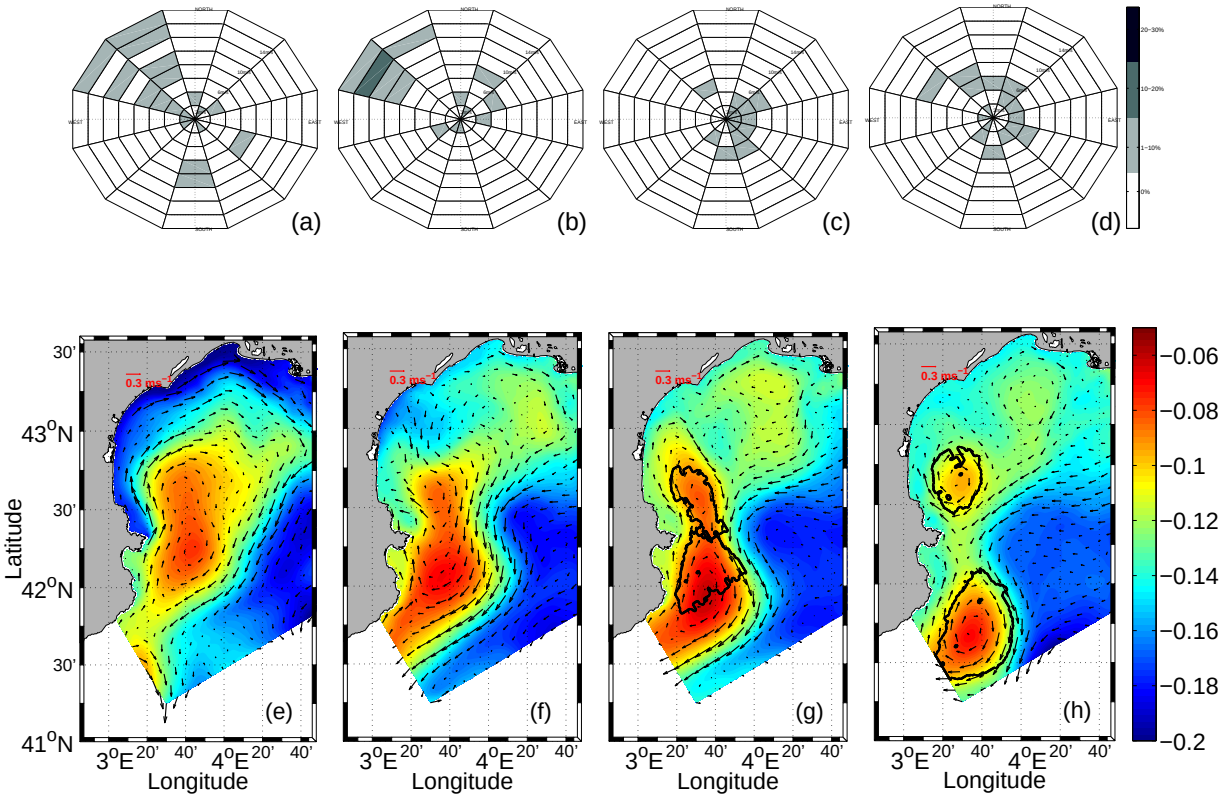

Figure 6. Time sequence of the generation process of *A2-Latex09* in 2009. Top: wind rose representation (intensity and frequency) at station Leucate on (a) 2009/07/18 to 20; (b) 2009/08/06 to 08; (c) 2009/08/14 to 16; (d) 2009/08/25 to 27; colors representing wind frequency (%). Bottom: sea surface height [m] and current velocity field at 5 m depth on (e) 2009/07/20; (f) 2009/08/08; (g) 2009/08/16; (h) 2009/08/27. Black contours in (g) and (h) show the eddies identification issued from the wavelet analysis.

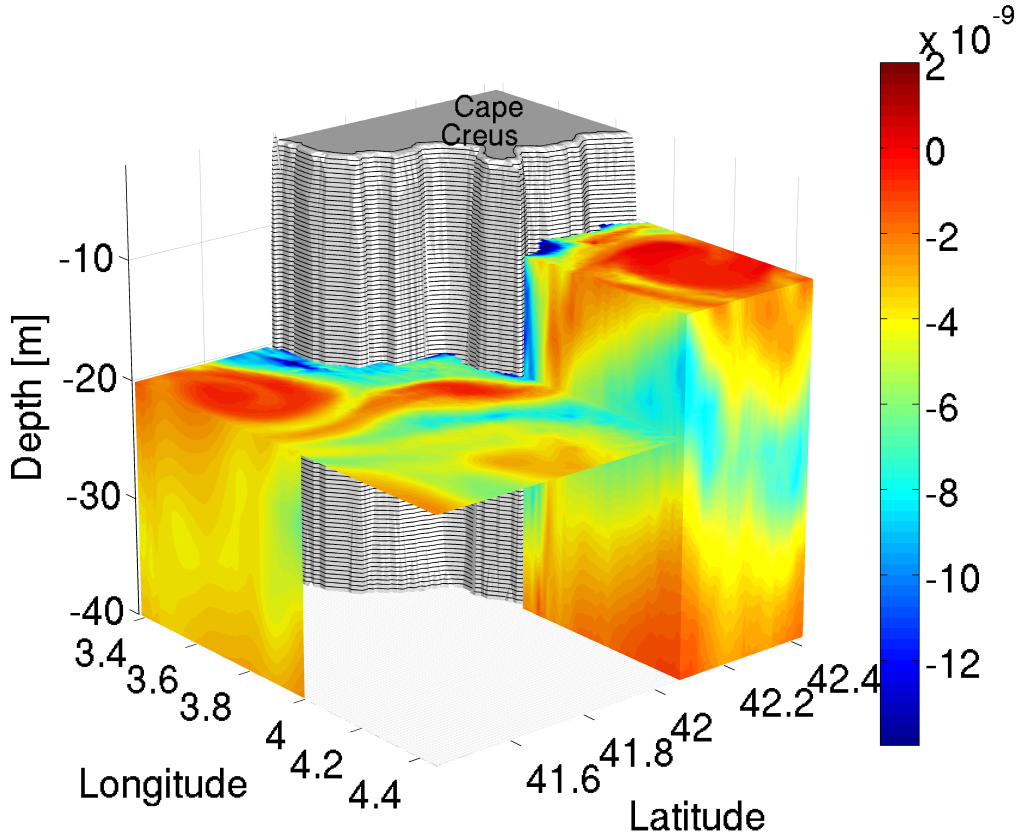

Figure 7. 3-dimensional sections of potential vorticity [kg m^{-4} s^{-1}] in color on September 3. The coast is represented in gray with the position of the Cape Creus. At 10 m depth, in the first section, we can distinguish the presence of A2-Latex09 upstream the Cape Creus. In the lee of the Cape, the transient structure is evidenced at 20 m depth. The Catalan eddy is also visualized farther off the coast and until 40 m depth.

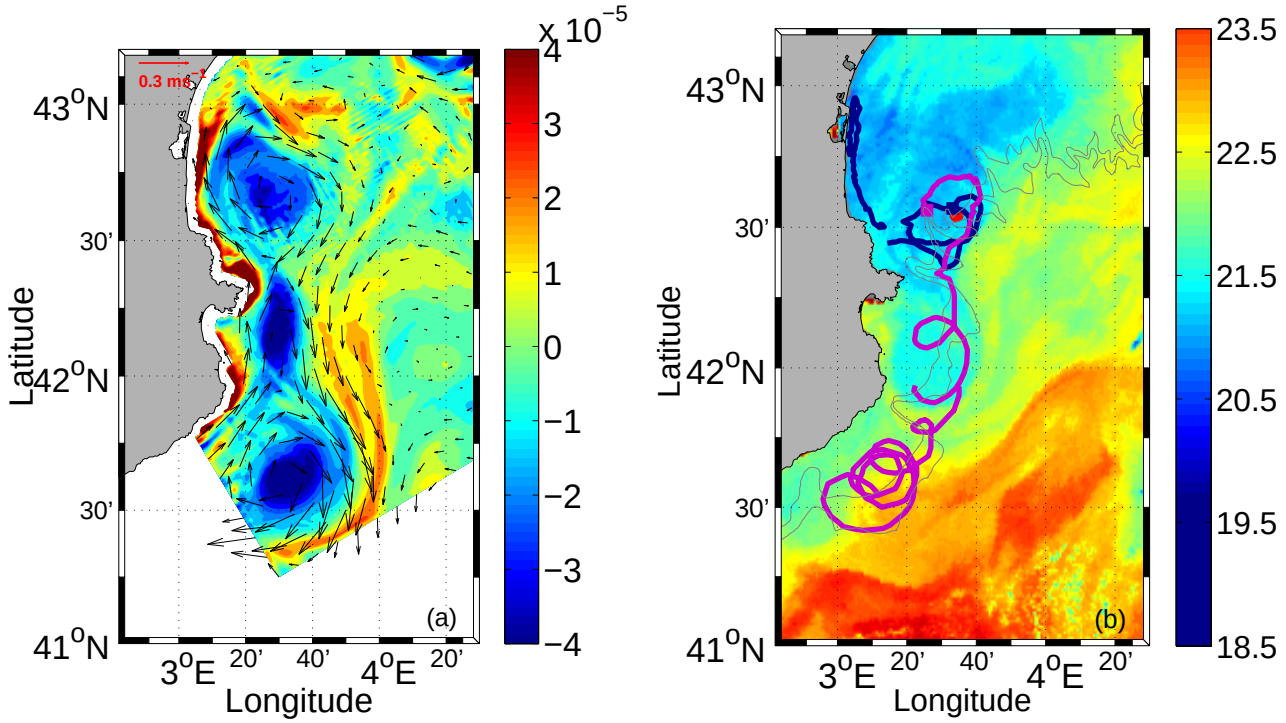

Figure 8. (a) Modeled relative vorticity [s^{-1}] and current velocity field at 20 m depth on September 3. (b) SST_b satellite image on August 28 (data from Météo-France) and drifter trajectories (drifter No. 83631 in blue - drifter No. 83632 in purple) from August 26 to September 12. The squares represent the drifters' initial positions. The red dot corresponds to the eddy center.